

On-Chip GaAs-Based Spoof Surface Plasmon Polaritons at Millimeter-Wave Regime

Kai-Da Xu¹, Senior Member, IEEE, Ying-Jiang Guo², Qian Yang³, Yong-Liang Zhang⁴, Member, IEEE, Xianjin Deng, Anxue Zhang⁵, and Qiang Chen⁶, Senior Member, IEEE

Abstract—In this letter, a GaAs-based wideband spoof surface plasmon polariton (SSPP) waveguide with super compact size is presented at millimeter-wave regime. The periodic SSPP unit cell consists of a longitudinal slot and a meander slot in transversal direction, and its corresponding waveguide has good low-pass filtering feature. The momentum of microstrip line for measurement feeding to the SSPPs can be well matched without any gradient transition structures. To apply this SSPP waveguide into the design of bandpass filter (BPF), a row of vias is added with a certain distance from the SSPP unit cells. For demonstration, two on-chip examples, i.e., SSPP waveguide and SSPP-based BPF, are fabricated operating at different frequencies. Good agreement between simulations and measurements validates the propagation characteristics and implementation of the proposed SSPPs.

Index Terms—Bandpass filter, millimeter-wave, on-chip devices, spoof surface plasmon polaritons, waveguide.

I. INTRODUCTION

SURFACE plasmon polaritons (SPPs) are classic surface electromagnetic waves in optical bands [1], which have been widely used in sensing and modulating [2]–[4]. In 2004, a periodic metal hole array supporting SPP-like surface mode was proposed with strong field confinement in the lower frequencies [5], named as designer or spoof SPPs (SSPPs). This expands the advantages of SPPs from optical regime to microwave or terahertz bands, therefore, SSPPs have been developed utilizing various periodically structured arrays from then on [6], [7]. Meanwhile, numerous SSPPs have been applied in the design of different devices in the past

Manuscript received November 24, 2020; revised January 19, 2021; accepted January 25, 2021. Date of publication January 27, 2021; date of current version February 5, 2021. This work was supported in part by the FY2019 Japan Society for the Promotion of Science (JSPS) Postdoctoral Fellowship for Research in Japan under Grant P19350 and in part by the Grant-in-Aid for JSPS Research Fellow under Grant JP19F19350. (Corresponding author: Ying-Jiang Guo.)

Kai-Da Xu is with the School of Information and Communications Engineering, Xi'an Jiaotong University, Xi'an 710049, China, and also with the Department of Communications Engineering, Tohoku University, Sendai 980-8579, Japan.

Ying-Jiang Guo and Xianjin Deng are with the Microsystem and Terahertz Research Center, China Academy of Engineering Physics, Chengdu 610200, China (e-mail: guoyingjiang1@gmail.com).

Qian Yang and Anxue Zhang are with School of Information and Communications Engineering, Xi'an Jiaotong University, Xi'an 710049, China.

Yong-Liang Zhang is with the College of Transportation, Inner Mongolia University, Hohhot 010024, China.

Qiang Chen is with the Department of Communications Engineering, Tohoku University, Sendai 980-8579, Japan.

Color versions of one or more figures in this letter are available at <https://doi.org/10.1109/LPT.2021.3054962>.

Digital Object Identifier 10.1109/LPT.2021.3054962

decade [8]–[20], including bandpass filters (BPFs) [8]–[14], antennas [15]–[17], sensors [18] and splitters [19], [20].

In order to facilitate the measurements and effectively excite the SSPP modes, a matching transition is needed with mode conversion from traditional guided waves to SSPPs. For instance, in [8], a broadband BPF based on SSPPs was proposed, with a flaring ground as the matching transition from coplanar waveguide to SSPP waveguide. However, this method will sacrifice a large occupation in transversal direction. In [9], [10], a balun was utilized to match the mode conversions from microstrip lines to SSPPs, but it would inevitably increase the design complexity of the SSPP-based BPFs. Hence, how to simplify the matching transition topologies of the SSPP-based devices with compact sizes and highly efficient mode conversions is still technically challenging.

On the other hand, most of the above-mentioned works were operated in microwave frequencies using the standard printed circuit board fabrication process. However, few works on SSPPs were experimentally investigated at higher frequencies, such as millimeter-wave and terahertz regimes, using integrated circuit process. In [21], an on-chip BiCMOS based SSPP transmission line in sub-terahertz regime was presented, but only transmission characteristics of the SSPPs was demonstrated, without any device applications. In our previous work [22], a millimeter-wave on-chip BPF based on SSPPs was proposed with low coupling feature, however, its transversal size needs to be further reduced for the application in integrated circuits.

In this letter, a new GaAs-based wideband SSPP waveguide with super compact size is presented. The asymptotic frequency of the SSPP unit cell at millimeter-wave regime can be easily controlled. Moreover, the momentum of microstrip line for measurement feeding to the proposed SSPPs can be well matched without adding any gradient transition structures. Then, the proposed SSPP waveguide can be applied into the design of BPF, whose left and right edges of the passband can be also adjusted. Finally, a brief conclusion is given.

II. MEANDER SLOT BASED SSPP WAVEGUIDE

A. Proposed SSPP Unit Cell

Fig. 1(a) shows the stack-up of the standard 0.15- μm GaAs PHEMT technology. The periodic SSPP unit cell is designed on M1 layer, which consists of a longitudinal slot and a meander slot to miniaturize the circuit size in transversal direction,

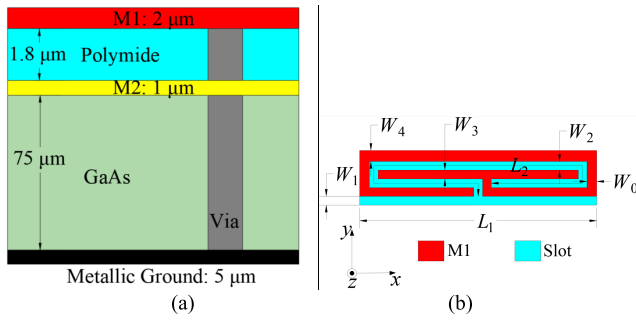


Fig. 1. (a) Stack-up of the employed 0.15- μm GaAs PHEMT technology, where the GaAs and polymide films have the relative permittivities of 12.9 and 2.9, respectively. Two metal layers M1 and M2 are available for circuit design, with conductivity of $4 \times 10^7 \text{ S/m}$. (b) Proposed SSPP unit cell using a longitudinal slot and a meander slot in transversal direction, where $L_1 = 355 \mu\text{m}$, $L_2 = 690 \mu\text{m}$, $W_0 = 10 \mu\text{m}$, $W_1 = 2.5 \mu\text{m}$, $W_2 = 5 \mu\text{m}$, $W_3 = 10 \mu\text{m}$, and $W_4 = 17.5 \mu\text{m}$.

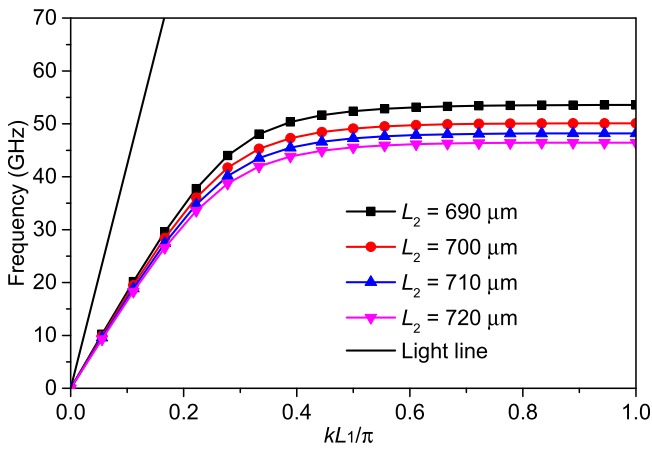


Fig. 2. Dispersion characteristics of the proposed SSPP waveguide against different values of L_2 . The parameter k in the figure is the propagation constant.

as illustrated in Fig. 1(b). The lengths of the longitudinal slot and meander slot are L_1 and L_2 , and their widths are W_1 and W_2 , respectively. The width of all metal strips is set as W_0 , except the one wrapped by the meander slot and the outermost longitudinal one, whose widths are W_3 and W_4 , respectively. When the length of L_2 and width of W_2 are changed, the width of W_3 will be tuned accordingly. The matching from the microstrip line to SSPP waveguide can be optimized by changing the width of the outermost longitudinal metal strip W_4 , which will be analyzed in the next sub-section.

In order to investigate the propagation characteristics of the SSPPs, the dispersion curves are simulated using the commercial software CST Microwave Studio. Fig. 2 shows the simulated dispersion characteristics of the proposed SSPP waveguide against different values of parameter L_2 , while maintaining other parameters unchanged except W_3 . Due to the layout arrangement in Fig. 1(b), as the parameter L_2 is changed from $690 \mu\text{m}$ to $720 \mu\text{m}$ with the step of $10 \mu\text{m}$, the parameter W_3 will be increased from $10 \mu\text{m}$ to $25 \mu\text{m}$ with the step of $5 \mu\text{m}$ accordingly.

Seen from Fig. 2, an apparent deviation between the dispersion curve and light line can be observed, which indicates

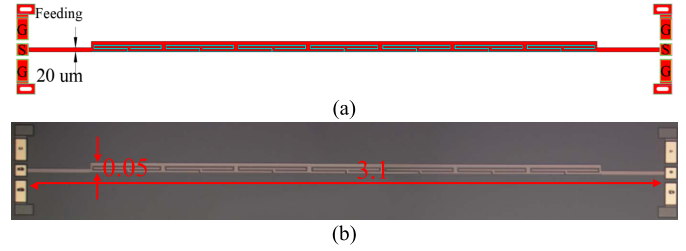


Fig. 3. (a) Topology of the SSPP waveguide, and (b) its fabricated die photograph (unit: mm).

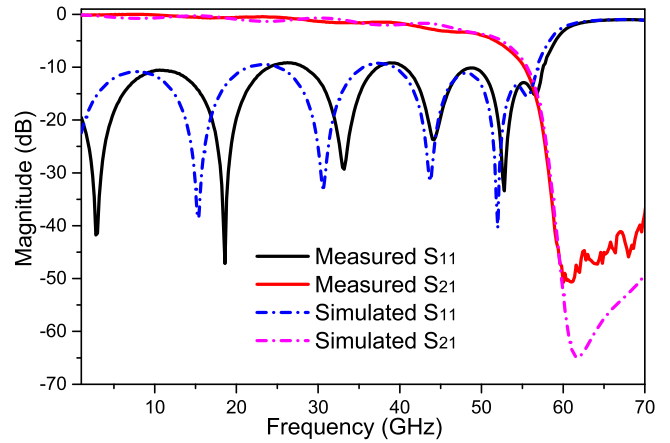


Fig. 4. Simulated and measured S-parameters of the proposed SSPP waveguide.

that the structure has a strong confinement ability of the electromagnetic wave on the surface. Moreover, the asymptotic frequency can be easily tuned by changing the length of the meander slot. As the slot length L_2 increases, larger deviation from light line and lower asymptotic frequency occur.

B. SSPP Waveguide

Based on the above dispersion feature, a corresponding SSPP waveguide consisting of seven SSPP unit cells is designed with low-pass filtering property. As shown in Fig. 3(a), a microstrip line is directly connected to the proposed SSPPs for measurement feeding with ground-signal-ground (GSG) probing pads at the input/output ports. Therefore, the whole topology only consists of two parts, input/output feeding part using GSG pads with a section of microstrip line and the periodic array of the proposed SSPP unit cells. The width of the microstrip line is set as $20 \mu\text{m}$, and other dimensions of SSPP waveguide are the same as those of SSPP unit cell in Fig. 1(b). Fig. 3(b) illustrates the die photograph of the fabricated SSPP waveguide, where the overall size is $3.1 \text{ mm} \times 0.05 \text{ mm}$.

The momentum of microstrip line to the proposed SSPPs is well matched even if there is no any gradient transition structure, which can be verified from the S-parameter simulations and measurements. The on-chip SSPP waveguide is measured via an on-wafer GSG probing with the help of a vector network analyzer. As seen in Fig. 4, the cut-off frequency of the SSPP waveguide is at around 54 GHz, consistent with the asymptotic

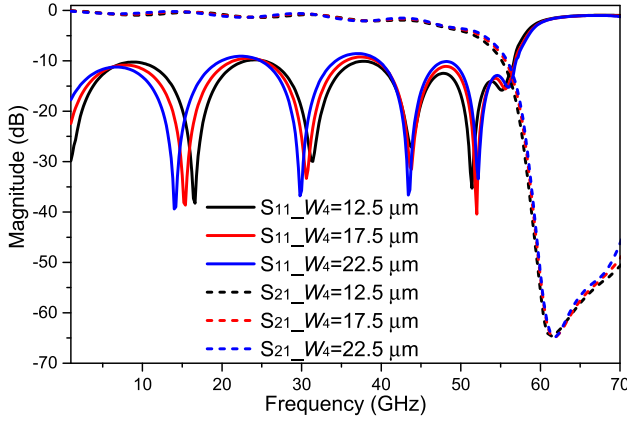


Fig. 5. In-band impedance matching adjustment of the SSPP waveguide with different values of W_4 .



Fig. 6. Topology of the proposed BPF, where $H_1 = 415 \mu\text{m}$, $d_1 = 70 \mu\text{m}$, $d_2 = 120 \mu\text{m}$, and $L_0 = 400 \mu\text{m}$.

frequency in Fig. 2 when $L_2 = 690 \mu\text{m}$. Good agreement between the simulated and measured results has been realized, possessing an excellent low-pass filtering performance for a millimeter-wave on-chip device.

Although there is no gradient transition structure from the microstrip line to SSPPs, the in-band impedance matching is still maintained in a good level. Moreover, it can be also slightly optimized by tuning the width of the outermost longitudinal metal strip W_4 , as illustrated in Fig. 5.

III. MILLIMETER-WAVE BPF APPLICATION

Furthermore, the proposed SSPP waveguide can be applied in the design of BPF through adding a row of vias with a certain distance from the SSPP unit cells, as shown in Fig. 6. Except the via structure, the unit cell topology is similar to that of SSPP unit cell in Fig. 1(b), but their dimensions are different. To realize a higher cut-off frequency (i.e., right edge) of the passband, a larger asymptotic frequency of SSPPs is needed. Herein, the dimensions of the proposed SSPP unit cells are set as $L_1 = 284 \mu\text{m}$, $L_2 = 516 \mu\text{m}$, $W_0 = 18 \mu\text{m}$, $W_1 = 10 \mu\text{m}$, $W_2 = 12 \mu\text{m}$, $W_3 = 18 \mu\text{m}$. The remaining dimensions of the microstrip feeding and via distance can be seen in the caption of Fig. 6.

For this BPF, the left and right edges of the passband can be tuned by the parameters H_1 and L_2 , as shown in Fig. 7(a) and 7(b), respectively. Thus, the center frequency and bandwidth of the BPF can be controlled accordingly. Note that there is a trade-off between the bandwidth and the circuit size in transversal direction, since the bandwidth will be broadened as the parameter H_1 increases, at the expense of the transversal size of the BPF circuit.

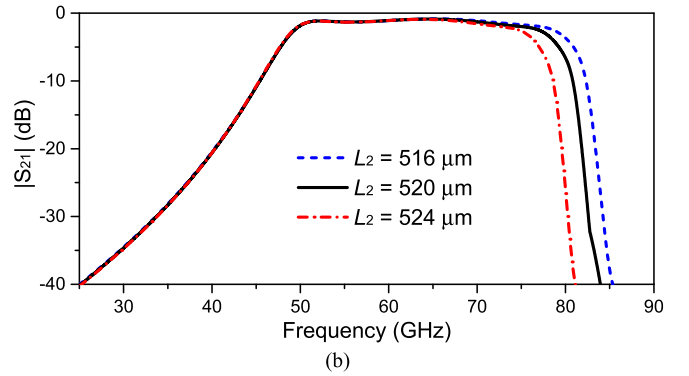
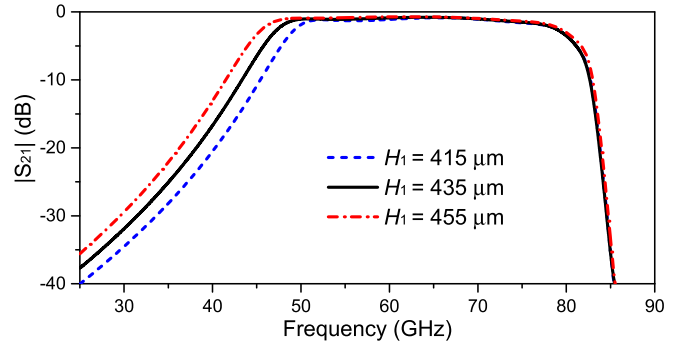


Fig. 7. Simulated passband adjustment with different values of (a) H_1 and (b) L_2 .

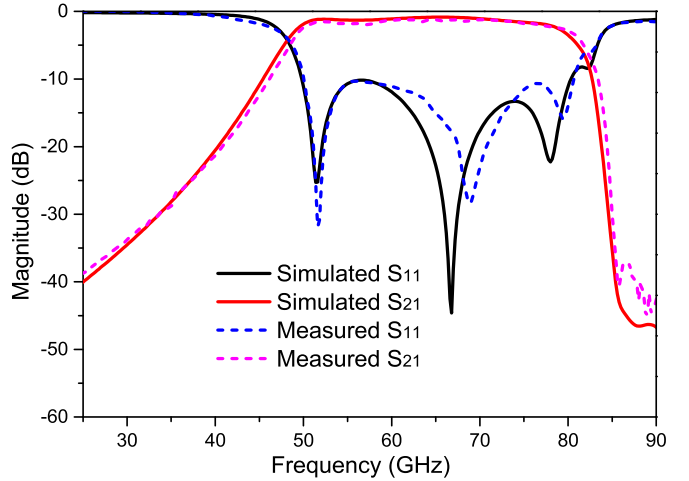


Fig. 8. Simulated and the measured results of the BPF.



Fig. 9. Fabricated die photograph (unit: mm).

Fig. 8 shows the simulated and measured S-parameters of the proposed BPF, where the center frequency is at 65 GHz with 3-dB fractional bandwidth of 50.5% (48.6 ~ 81.4 GHz). The simulation and measurement results agree reasonably well with each other. The measured insertion losses are at the range

between 1.4 and 2.0 dB within the passband, and the measured return losses are better than 11 dB. The fabricated die photo of the millimeter-wave BPF is shown in Fig. 9, whose size is 2.5 mm × 0.47 mm.

IV. CONCLUSION

A super compact GaAs-based wideband SSPP waveguide is presented, whose asymptotic frequency at millimeter-wave regime is easily manipulated by the meander slot. A direct connection of the SSPP waveguide with microstrip line for measurement is realized, which simplifies the design. To apply the proposed SSPPs into the design of BPF, a row of vias is employed. Consequently, a millimeter-wave on-chip BPF is implemented with tunable center frequency and bandwidth. Good agreements between the simulated and measured results validate the proposed idea.

REFERENCES

- [1] W. L. Barnes, A. Dereux, and T. W. Ebbesen, "Surface plasmon sub-wavelength optics," *Nature*, vol. 424, no. 6950, pp. 824–830, Aug. 2003.
- [2] K. A. Willets and R. P. Van Duyne, "Localized surface plasmon resonance spectroscopy and sensing," *Annu. Rev. Phys. Chem.*, vol. 58, pp. 267–297, May 2007.
- [3] Y. Liang, W. Cui, L. Li, Z. Yu, W. Peng, and T. Xu, "Large-scale plasmonic nanodisk structures for a high sensitivity biosensing platform fabricated by transfer nanoprinting," *Adv. Opt. Mater.*, vol. 7, no. 7, 2019, Art. no. 1801269.
- [4] Y. Yuan *et al.*, "Independent phase modulation for quadruplex polarization channels enabled by chirality-assisted geometric-phase metasurfaces," *Nature Commun.*, vol. 11, no. 1, pp. 1–9, Dec. 2020.
- [5] J. B. Pendry, "Mimicking surface plasmons with structured surfaces," *Science*, vol. 305, no. 5685, pp. 847–848, Aug. 2004.
- [6] C. R. Williams, S. R. Andrews, S. A. Maier, A. I. Fernández-Domínguez, L. Martín-Moreno, and F. J. García-Vidal, "Highly confined guiding of terahertz surface plasmon polaritons on structured metal surfaces," *Nature Photon.*, vol. 2, pp. 175–179, Mar. 2008.
- [7] X. Shen, T. J. Cui, D. Martín-Cano, and F. J. García-Vidal, "Conformal surface plasmons propagating on ultrathin and flexible films," *Proc. Nat. Acad. Sci. USA*, vol. 110, no. 1, pp. 40–45, Jan. 2013.
- [8] L. Zhao *et al.*, "A novel broadband band-pass filter based on spoof surface plasmon polaritons," *Sci. Rep.*, vol. 6, no. 1, p. 36069, Oct. 2016.
- [9] K.-D. Xu, F. Zhang, Y.-J. Guo, L. Ye, and Y. Liu, "Spoof surface plasmon polaritons based on balanced coplanar stripline waveguides," *IEEE Photon. Technol. Lett.*, vol. 32, no. 1, pp. 55–58, Jan. 1, 2020.
- [10] Y. Guo, K. D. Xu, Y. Liu, and X. Tang, "Novel surface plasmon polariton waveguides with enhanced field confinement for microwave-frequency ultra-wideband bandpass filters," *IEEE Access*, vol. 6, pp. 10249–10256, 2018.
- [11] Y. J. Guo, K. D. Xu, and X. Tang, "Spoof plasmonic waveguide developed from coplanar stripline for strongly confined terahertz propagation and its application in microwave filters," *Opt. Exp.*, vol. 26, no. 8, pp. 10589–10598, Apr. 2018.
- [12] K. D. Xu, Y. J. Guo, and X. Deng, "Terahertz broadband spoof surface plasmon polaritons using high-order mode developed from ultra-compact split-ring grooves," *Opt. Exp.*, vol. 27, no. 4, pp. 4354–4363, Feb. 2019.
- [13] J. Li, J. Shi, K.-D. Xu, Y.-J. Guo, A. Zhang, and Q. Chen, "Spoof surface plasmon polaritons developed from coplanar waveguides in microwave frequencies," *IEEE Photon. Technol. Lett.*, vol. 32, no. 22, pp. 1431–1434, Nov. 15, 2020.
- [14] K.-D. Xu, S. Lu, Y.-J. Guo, and Q. Chen, "High-order mode of spoof surface plasmon polaritons and its application in bandpass filters," *IEEE Trans. Plasma Sci.*, vol. 49, no. 1, pp. 269–275, Jan. 2021.
- [15] W. Feng, Y. Feng, W. Yang, W. Che, and Q. Xue, "High-performance filtering antenna using spoof surface plasmon polaritons," *IEEE Trans. Plasma Sci.*, vol. 47, no. 6, pp. 2832–2837, Jun. 2019.
- [16] Q. L. Zhang, B. J. Chen, Q. Zhu, K. F. Chan, and C. H. Chan, "Wideband millimeter-wave antenna with low cross polarization based on spoof surface plasmon polaritons," *IEEE Antennas Wireless Propag. Lett.*, vol. 18, no. 8, pp. 1681–1685, Aug. 2019.
- [17] W. Feng, Y. Feng, L.-S. Wu, Y. Shi, X. Y. Zhou, and W. Che, "A novel leaky wave endfire filtering antenna based on spoof surface plasmon polaritons," *IEEE Trans. Plasma Sci.*, vol. 48, no. 7, pp. 3061–3066, Sep. 2020.
- [18] Y.-J. Guo, K.-D. Xu, and X. Deng, "Tunable enhanced sensing of ferrite film using meander-shaped spoof surface plasmon polariton waveguide," *Appl. Phys. Exp.*, vol. 12, no. 11, Nov. 2019, Art. no. 115502.
- [19] X. Gao *et al.*, "Ultrathin dual-band surface plasmonic polariton waveguide and frequency splitter in microwave frequencies," *Appl. Phys. Lett.*, vol. 102, no. 15, Apr. 2013, Art. no. 151912.
- [20] J. Wang, L. Zhao, Z. C. Hao, X. P. Shen, and T. J. Cui, "Splitting spoof surface plasmon polaritons to different directions with high efficiency in ultra-wideband frequencies," *Opt. Lett.*, vol. 44, no. 13, pp. 3374–3377, Jul. 2019.
- [21] Z. Qi, X. Li, and H. Zhu, "Low-loss BiCMOS spoof surface plasmon polariton transmission line in sub-THz regime," *IET Microw., Antennas Propag.*, vol. 12, no. 2, pp. 254–258, 2018.
- [22] Y.-J. Guo, K.-D. Xu, X. Deng, X. Cheng, and Q. Chen, "Millimeter-wave on-chip bandpass filter based on spoof surface plasmon polaritons," *IEEE Electron Device Lett.*, vol. 41, no. 8, pp. 1165–1168, Aug. 2020.